Saleh et al., Geoinfor Geostat: An Overview 2020, 8:5
DOI: 10.37532/gigs.2020.8(5).269

Geoinformatics & Geostatistics: An Overview

Research Article

A SCITECHNOL JOURNAL

Effectively Using Multispectral Remote Sensing and GIS Techniques for Precision Radioactive Mineral Exploration in Um Ara – Um Shilman Area, South Eastern Desert of Egypt

Gehad M. Saleh*, Reda A. El-Arafy and Mohamed S. Kamar

Abstract

Um Ara-Um Shilman younger granites are one of the most promising uranium and thorium mineralization in the south Eastern Desert of Egypt. These granites are classified into monzogranite and alkali-feldspar granite. The using of remote sensing image processing techniques and Geographic Information Systems (GIS), considered an effective, powerful tool in the field of lithologic mapping and mineral exploration lately. Landsat 8 Operational Land Imager OLI showed a great capability in geologic exploration, especially for the remote and high terrain areas, reducing time and efforts at Um Ara – Um Shilman area. The results showed a distinctive differentiation between the different lithologies rocks unites especially fine to medium-grained alkali feldspar fertile granite and coarse-grained monzogranite. The northern location has gained more attention regarding its radioactive anomaly recorded in the medium to fine grained granitic variety that range in composition from alibied to the k-feldspar-rich granite. Radioelements measurements (equivalent uranium (eU) ppm, equivalent thorium (eTh) ppm, potassium percent (K%) and total count (Tc)) have been acquired from sixteen trenches covered the northern locality of the study area. These trenches can be classified into two groups; the first one is high in uranium and the second is high in thorium, and the uranium migrated from the eastern part to the western part of the study area. GIS methods are successful and has a great advantage to apply in a ground radioelements measurement for a local investigation area. The results of the study indicated a significant value for further future radioactive exploration in the area.

Keywords

Image processing; Landsat 8 OLI; PCA; Uranium mineralization; GIS; Um Ara; Egypt

Introduction

The Eastern Desert (ED) of Egypt is divided into three sectors; Northern, Central and Southern sectors. These divisions confine parts with common geographic and litho-structural discontinuities [1]. The South Eastern Desert (SED) is largely occupied by Gneissic and migmatite rocks with a more complex shape rarely associated with remnants of older granites.

The granitic rocks in the Eastern Desert of Egypt were classified as; syn- to late-orogenic granitoids (Older granitoids) and post-orogenic to anorogenic granites (Younger granites) [2,3]. The older granitoids range in composition from quartz diorite to rare true granite (predominantly muscovite trondhjemite, tonalite, and granodiorite). They are I-type, subduction-related plutons, with ages between 870 and 614 Ma using Rb-Sr and U-Pb methods [4,5]. Younger granites are mainly monzogranites, syenogranites, and alkali-feldspar granites, I-type (partly subduction-related) but mainly alkaline to peralkaline A-type plutons, formed between 610 and 550 Ma based on the Rb-Sr and U-Pb dating [6], and developed during extensional processes.

The granitic rocks, especially those of felsic nature and younger ages, are generally considered as one of the most important uranium mineralization either directly or indirectly. The direct sources are founded when the U-mineralization are mainly formed from the aqueous fluids accumulated during the late stages of magmatic differentiation. On the other hand, the indirect sources are mostly related to post magmatic redistribution of uranium as they are of secondary origin.

Nuclear Materials Authority (NMA) started a wide comprehensive exploration program to search for uranium deposits in Egypt. These programs led to discovery of radioactive anomalies and uranium mineralization in the Northern (Gabal (G.) Gattar), Central (G. El Missikat and G. El Erediya) and Southern (G. Um Ara and G. El-Sella) Eastern Desert of Egypt. The area under investigation lies in the SED between latitudes 22° 31` N - 22° 41`N, and longitudes 33° 48`E – 33° 54`E (Figure 1).

Remote sensing images are widely used for geological and/or mineralogical mapping using their spectral signatures. It has the ability to detect the alteration zones by its spectral characteristics such as iron, hydroxyl, sulphate, and carbonate- bearing minerals. Landsat 8 Operational Land Imager (OLI) data can detect the altered rocks and ferrous minerals due to the distinctive absorption and reflectance characteristics of these rocks and their mineral content. Several studies have demonstrated the utility of remotely sensed data for geological mapping and lithologic identification. The spectral features detected in rocks from the visible through shortwave infrared (0.4-2.5 μm) portions of the electromagnetic spectrum, are mainly due to iron oxide, carbonate and hydroxyl-bearing minerals, while silicate minerals exhibit spectral feature in the thermal infrared TIR [7-16].

The objective of this research study is to test and analyse the best remote sensing algorithms using Landsat 8 (OLI) for discrimination the possible radioactive zones of interest in the area of Um Ara – Um Shilman at the SED of Egypt, which will assist in the further mineral exploration and evaluation studies in future. In addition, GIS techniques were applied to the measured spectrometry data that were collected locally over the northern part of the Um Ara area, where the highest radioactive anomaly was previously detected by the Egyptian Nuclear Materials Authority. The common GIS interpolation and ratios techniques, used to be applied to airborne spectrometry data; however, this study represents the effective possibility to apply some of these techniques for a ground data acquisition

***Corresponding author:** Gehad M. Saleh, Professor of Economic Geology, Head of Research Sector of Geology Nuclear, Materials Authority, Cairo, Egypt. E-mail: drgehad_m@yahoo.com

Received: June 30, 2020 **Accepted:** September 06, 2020 **Published:** September 23, 2020

doi: 10.37532/gigs.2020.8(5).269

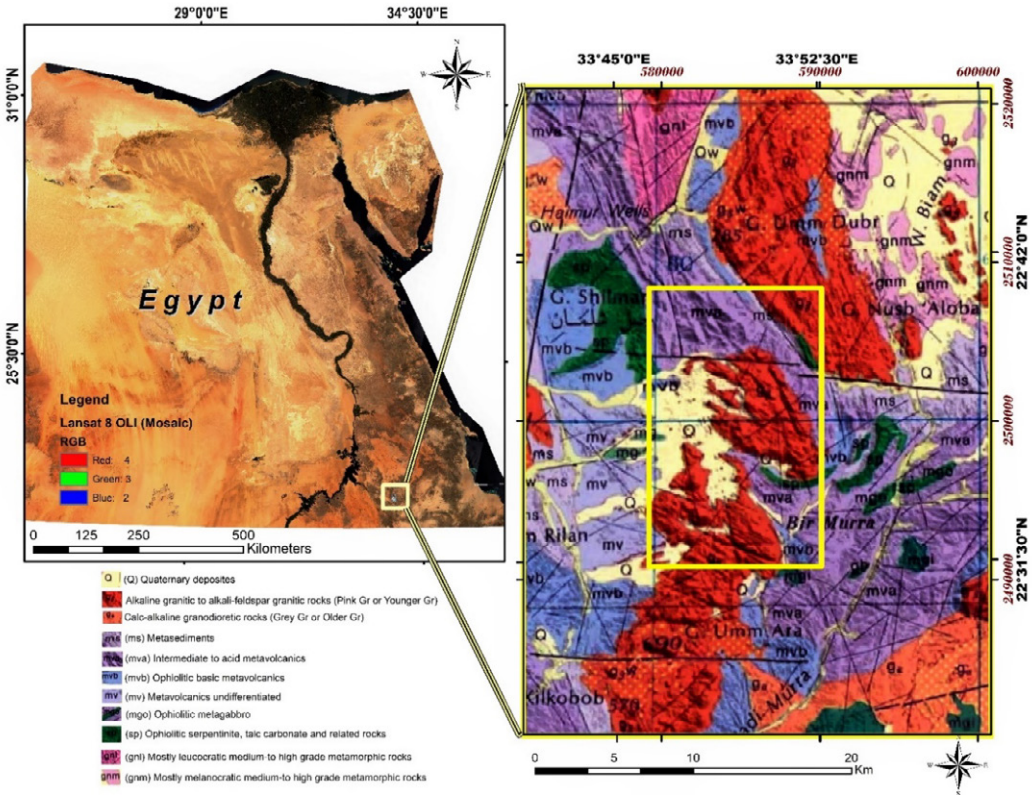

Figure 1: Mosaic satellite natural color image of Egypt (left) showing the location of the area of Um Ara – Um Shilman. General geologic map of the area (Right) modified after.

Geological Setting and Petrography

The geology of Um Ara - Um Shilman area has been extensively studied by many authors [17-20]. It comprises metavolcanics and Dokhan volcanism that were intruded by the Um Ara granites. These granites are classified into monzogranite and alkali-feldspar granite [20]. The monzogranite is an oval-shaped pluton trending N–S to NW–SE. It is a homogeneous and characterized by its pinkish colour, coarse-grained equigranularity texture and locally contains mafic xenoliths (10-20 cm in diameter). The alkali-feldspar granite is emplaced at the northern contact of Um Ara – Um Shilman monzogranite. It is fine to medium-grained, pinkish white or reddish-pink and red colours. It sends apophyses and off shoots (ranging in thickness from 1.5 cm to 250 m) into the northern Dokhan volcanic of G. Um Dubr [21]. The alkali-feldspar granite is affected by hydrothermal activities, which manifested by thematicization, silicification with partial kaolinization together with the frequent presence of manganese oxides, green and violet fluorite and uranium mineralization (uranophane and soddyite).

Petrographically, the monzogranite is composed essentially of quartz, plagioclase and k-feldspar (orthoclase and microcline) with subordinate amounts of biotite. Zircon and opaque minerals are the common accessories; while sericite, epidote and saussurite are presents as secondary minerals. Quartz is present as coarse-grained subhedral crystals commonly showing undulous extinction and contains inclusions of plagioclase. Plagioclase occurs as subordinate tabular crystals, which are partly to completely altered to saussurite and epidote (Figure 2a). It is twinned according to the Carlsbad-albite and albite laws and some crystals are zoned (Figure 2b). K-feldspars

Figure 2a: Photomicrograph of monzogranite showing plagioclase crystal partially saussuritized, Um Ara - Um Shilman area, (SED) of Egypt, (C. N.).

are represented by orthoclase and microcline forming subhedral to euhedral crystals rarely twinned which are turbid by sericite and clay minerals. Biotite occurs as small flakes filling the interstices between the plagioclase and k-feldspar crystals as well as some flakes are corroding plagioclase (Figure 2c). Zircon is present as euhedral short minute prismatic crystals up to 0.05 mm long, which enclosed within the quartz. Opaque minerals occur as small, scattered grains associating mostly the feldspar and quartz crystals.

The alkali-feldspar granite is composed mainly of k-feldspar, quartz, plagioclase, biotite and muscovite. Apatite, titanite and

doi: 10.37532/gigs.2020.8(5).269

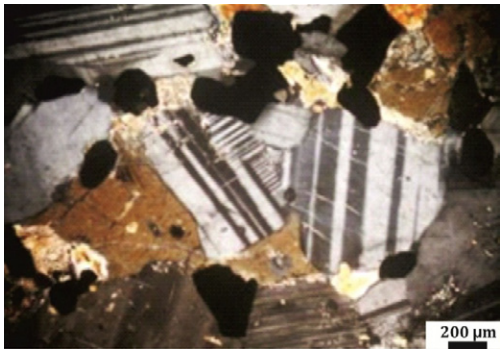

Figure 2b: Photomicrograph of monzogranite showing lamellar and percline twinning in plagioclase crystal, Um Ara - Um Shilman area, (SED) of Egypt, (C. N.).

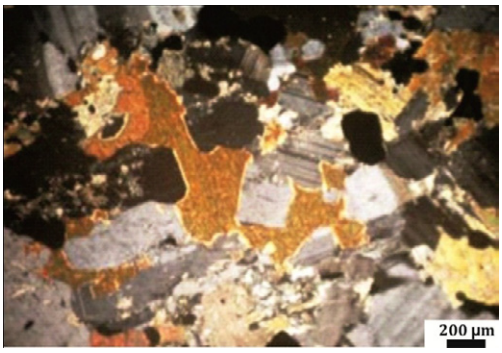

Figure 2c: Photomicrograph of monzogranite showing biotite flake corroded by plagioclase, Um Ara - Um Shilman area, (SED) of Egypt, (C. N.).

Figure 2d: Photomicrograph of alkali-feldspar granite showing graphic texture, Um Ara - Um Shilman area, (SED) of Egypt, (C. N.).

zircon are the most common accessory minerals; whereas sericite, kaolinite and epidote are the secondary ones. K-feldspars are composed mainly of orthoclase and microcline perthites. They occur as euhedral to subhedral crystals of string and patchy type perthites exhibiting secondary microclinization and albitization in local parts. Some perthite crystals are rimmed with albite. Quartz represents subhedral crystals occurs as interstitial grains between the other components, or as skeletal grains associating plagioclase and sometimes are assembling forming graphic-like texture (Figure 2d). Plagioclase occurs as euhedral to subhedral elongated crystals of albite to oligoclase in composition (An10-30) and exhibits albite and combined albite and pericline twinning. It exhibits partial saussuritization and shows albite and combined albite / Carlsbad twinning. Biotite occurs as euhedral to subhedral elongate to stubby flaky crystals. It is partly altered to chlorite and epidote. Muscovite is subhedral crystal and interstitial between feldspars but show marked local variations between the different subtypes. Apatite occurs as clear rod-like crystals enclosed in biotite (Figure 2e) and distinguished by low relief. Titanite occurs as euhedral rhombic-shaped crystals that are characterized by sphenoidal form (Figure 2f). Euhedral prismatic crystals of zircon enclosed within quartz and other minerals. Secondary uranium minerals (uranophane) occur as anhedral crystals associating plagioclase (Figure 2g).

Data and Methods

The dataset in this study consists of satellite Landsat 8 OLI (L1T) terrain corrected data for the entire area and Ground radioelements gamma-ray spectrometric measurements for 16 digs (trenches) at the northern part of the study area. Landsat 8 OLI data acquired on 29/1/2017 and geocoded to the UTM projection (WGS 84 – Zone 36 N). The chosen scene path and row are 173 and 44 respectively, with minimum cloud coverage (0.14%), covers the whole region; has been used in this study. Landsat 8 OLI L1T data are registered radiance-at-the-sensor product terrain corrected contains radiometrically calibrated and geometrically co-registered data. Four visible and near-infrared (VNIR) bands between 0.48 and 0.86 µm and two

Figure 2e: Photomicrograph of alkali-feldspar granite showing apatite included in biotite associating plagioclase, Um Ara - Um Shilman area, (SED) of Egypt, (C. N.).

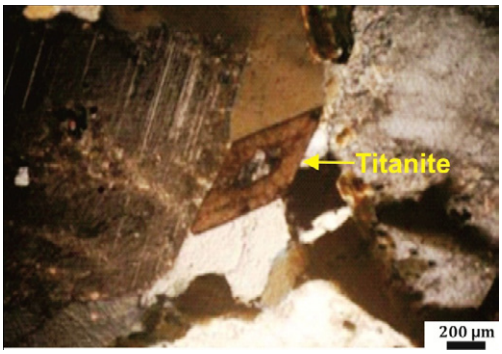

Figure 2f: Photomicrograph of alkali-feldspar granite showing well-formed crystal of titanite (sphene) associating plagioclase and quartz, Um Ara - Um Shilman area, (SED) of Egypt, (C. N.).

doi: 10.37532/gigs.2020.8(5).269

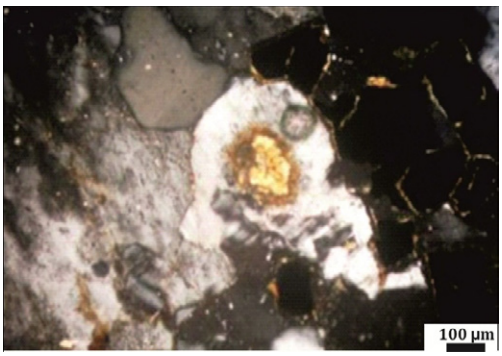

Figure 2g: Photomicrograph of alkali-feldspar granite showing cavity filled with uranophane accompanied by microclinization of plagioclase, Um Ara - Um Shilman area, South Eastern Desert (SED) of Egypt, (C. N.)

short-wave infrared (SWIR) bands from 1.6 to 2.2 µm, in addition to the coastal aerosol band at 044 µm, were stacked, resampled and registered to 15m resolution using the panchromatic band of (0.59 µm). All bands stacked forming 7 bands using the nearest neighbour method. All Landsat and spectrometry data analysis were carried out using the Environment for Visualizing Images (ENVI) and (ArcGIS) software. (Figure 3) shows the proposed flowchart used in this study.

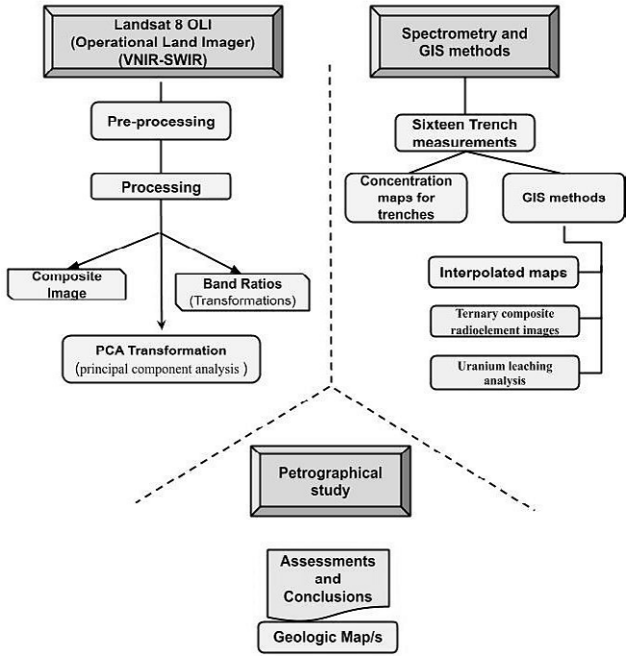

Figure 3: Flowchart of the proposed methods.

Landsat 8 OLI data

A pre-processing procedure has been applied for Landsat 8 OLI imagery, radiance data were atmospherically corrected and converted to surface reflectance using Fast Line-of-sight Atmospheric Analysis of Hypercubes (FLAASH). FLAASH is a first-principles atmospheric correction tool that corrects wavelengths in the visible through near-infrared and shortwave infrared regions, up to 3 µm.

The image processing techniques were used to represent spectral characteristics of the area of Um Ara – Um Shilman in terms of lithologic mapping and hydrothermal alterations distribution. An image enhancement was applied to the data by contrast stretching technique, in order to transform the multispectral image data format into an image display that either increases contrast between interesting targets and the background, or yields information about the composition of certain pixels in the image [10]. Colour composite, decorrelation stretching, band ratios and principle component analysis (PCA) were used in this research study.

Spectrometry measurements along trenches and GIS processing technique

The data were measured using a multichannel gamma-ray spectrometer model GS-256 with 3" X 3" (thallium activated) sodium iodide crystals. The sensors were calibrated over NMA calibration pads. The data are reported in four data channels: a) TC in (µr) : Total count (energy between 0.4 and 2.8 MeV), b) eU in (ppm): Equivalent Uranium (energy between 1.66 and 1.86 MeV), c) eTh in (ppm) : Equivalent Thorium (energy between 2.4 and 2.8 MeV) in ppm and d) K in percent (%): Potassium (energy between 1.37 and 1.57 MeV).

Each trench (nearly 5 meters in depth) with five faces; each face, measured in a grid pattern mapping format. The spatial mapping and relations methods were used the averages of radioelements measurements for every trench. For the average's value mapping purposes, an interpolation method named natural neighbour used for interpolate a raster surface from points in the GIS environments. Natural neighbour interpolation is a method developed by Sibson where it finds the closest subset of input samples to a query point and applies weights to them based on proportionate areas to interpolate a value [22]. In addition, radioelements ratios and pseudo colour composite image for both the radioelements and the ratios, were applied. The interpolation output was a raster, therefore the next step of making a composite image was to transform the raster output into grayscale image and used a chosen colour drape later in order to show the spatial variations and relations for the trenches' calculated average values.

Results and Discussion

In this research study, number of selected band ratios, bands composite images and PCA were applied to evaluate the discriminations of the lithologic units and the target radioactive alteration related zones. The second part of the study is focused on the north location of the Um Ara area, where a detailed investigation applied in the form of radioelements measurements from the dogged trenches.

Satellite image processing techniques

Landsat 8 OLI data can detect the altered rocks and ferrous minerals due to the absorption and reflectance characteristics of these rocks, which appear in the range of VNIR-SWIR.

Image Composite

A false colour composite (band 7, band 5 and band 3 in RGB) was generated for the purpose of lithological mapping (Figure 4). The image composite showed a distinctive discrimination between the major lithology's rock unites. Where alkali-feldspar granite appeared as a light brown colour, while monzogranite discriminated as dark brown colour. On the other hand, serpentinites are discriminated in blue colour, while metasediments in reddish colour. The composite

doi: 10.37532/gigs.2020.8(5).269

753 is considered very useful in lithologic discrimination and the additional enhancement can maximize the output benefits for the results.

Decorrelation stretching

The decorrelation stretching is an enhancement method apply to the image to remove the high correlation commonly found in the multispectral data sets and to produce a more colourful composite image with enhanced colour saturation. It is effectively improving the visual quality of the image spectral information, without significant distortion of its spectral characteristics. (Figure 4) shows the false colour composite image of bands 753 in RGB after applying the decorrelation stretching.

The process clearly showed the discrimination boundaries between the different mentioned rock unites particularly between the two type granites; alkali feldspar granite (brownish colour) and monzogranite (greenish colour). Also showed visibly the serpentinites, metasediments and dokhan volcanic as blue, purple and reddish colour respectively.

Band ratio (BR)

Band ratio is an image process produced by dividing the brightness digital number (DN) values at peaks and troughs in a reflectance curve, after removing the atmospheric conditions from the image such as haze. The band ratio method has the ability to show features that cannot be seen in the raw bands such as the hydrothermal alteration minerals. [23-26]. The band ratio 6/7 is very useful in mapping the clay minerals such as kaolinite and montmorillonite. The clay minerals are characterized by their high reflectance on band 6 and low in band 7. The band ratio 5/6 is used for mapping the ferrous minerals. The band ratio 4/2 is used for mapping the iron oxides which are of low reflectance in the red region and high absorption in the blue region of the electromagnetic wavelength. The results displayed in grayscale images (Figure 5).

Figure 6 showed the false colour composite image of the previously mentioned three band ratios as RGB image for lithological mapping and hydrothermal alteration [27]. This combination is clearly differentiating the alkali feldspar granite bodies as the darkest blue regions where the red arrows indicate the high potential radioactive zones as it discriminates clearly the fertile alkali-feldspar granite in the area

Principle Component Analysis (PCA)

PCA is a powerful statistical technique (a linear transformation) used to suppress irradiance effects and reduce redundancy in the multispectral images by transforming the original data onto new principal component axes which have a much higher contrast than the original bands. The output result of this process was uncorrelated PC bands equal to the number of the original bands the principal component images with moderate-to-high eigenvector loadings for diagnostic absorptive and reflective bands of the argillic-phyllic and oxide/hydroxide minerals, can be considered as the representative

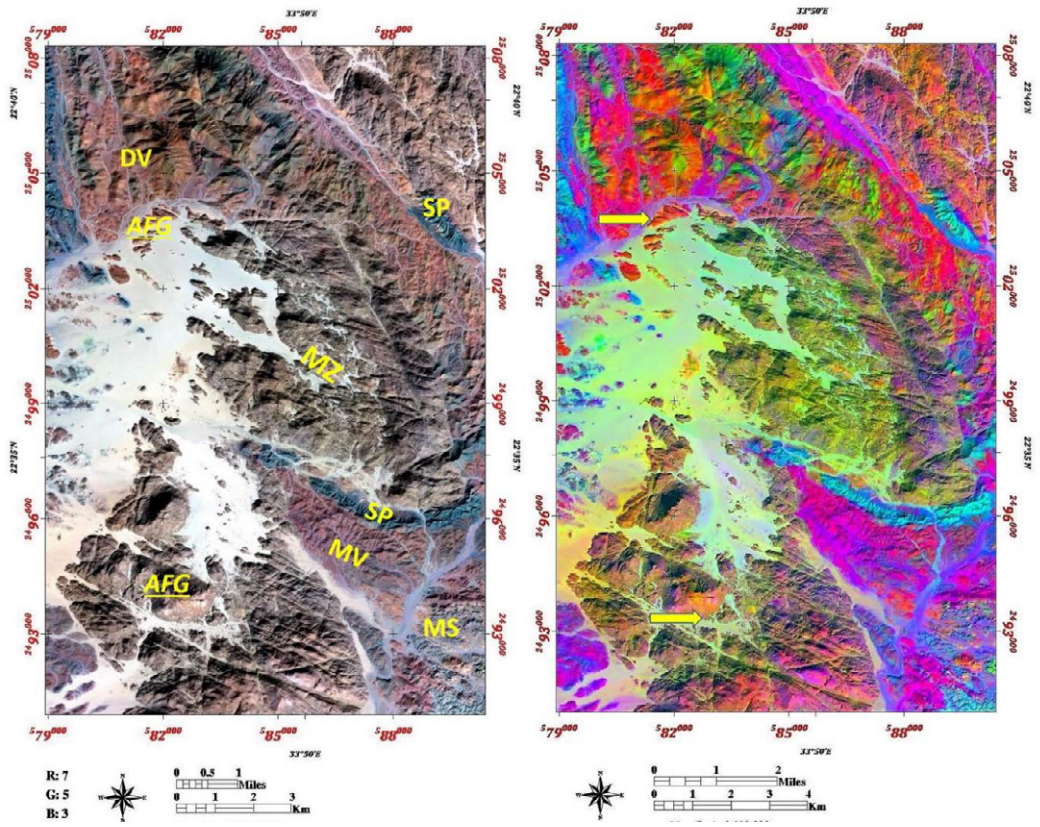

Figure 4: False color composite image bands 753 (left) and decorrelation stretch enhancement (right), showing the distinctive rock unit boundaries as: (MS) metasediments; (MV) metavolcanics; (SP) serpentinite; (DV) dokhanvolcanics; (MZ) monzogranite and (AFG) alkali-feldspar granite, Um Ara - Um Shilman area, (SED) of Egypt.

doi: 10.37532/gigs.2020.8(5).269

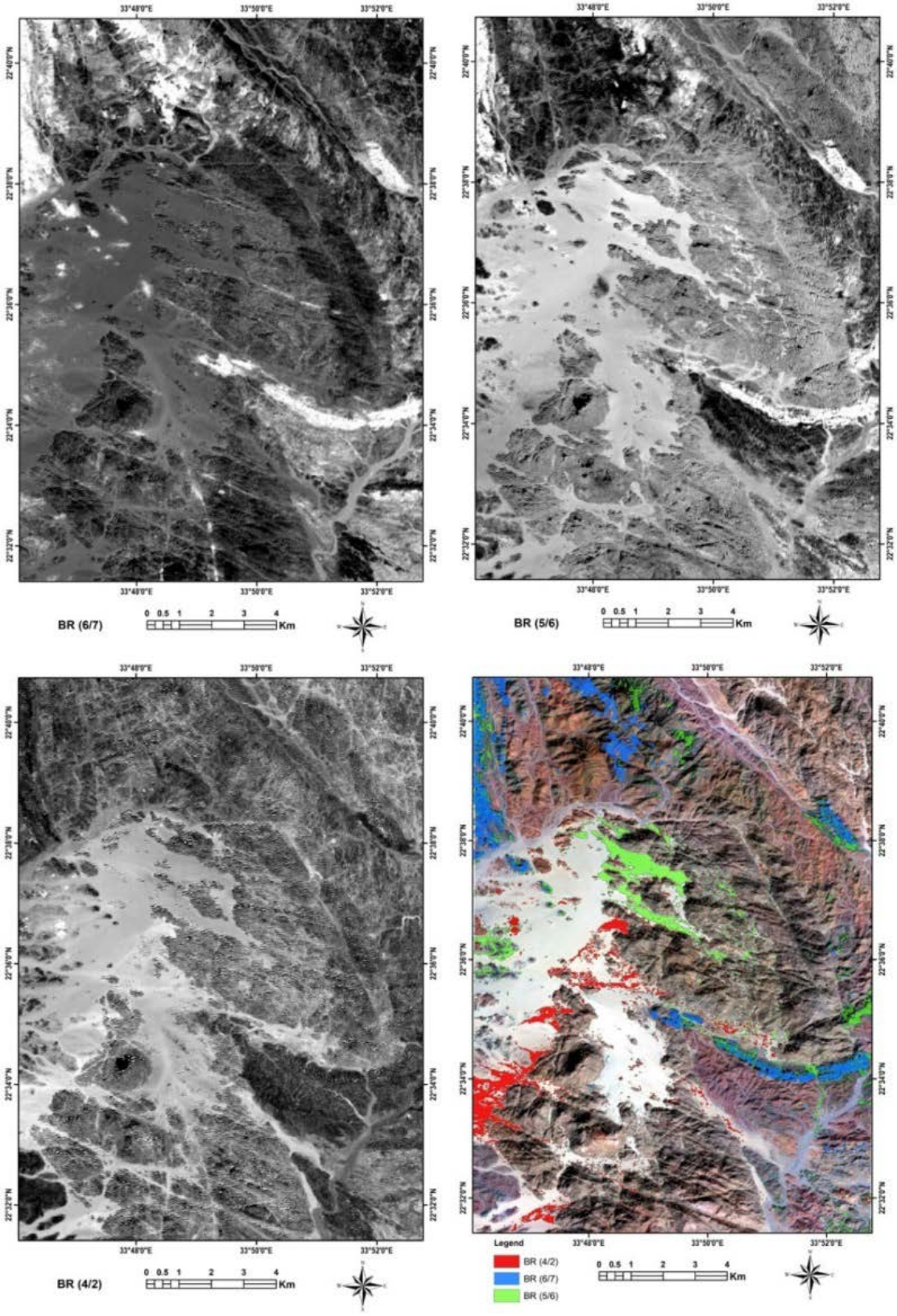

Figure 5: Band ratios in grayscale for (6/7), (5/6) and (4/2), and its density slices,Um Ara - Um Shilman area, (SED) of Egypt.

doi: 10.37532/gigs.2020.8(5).269

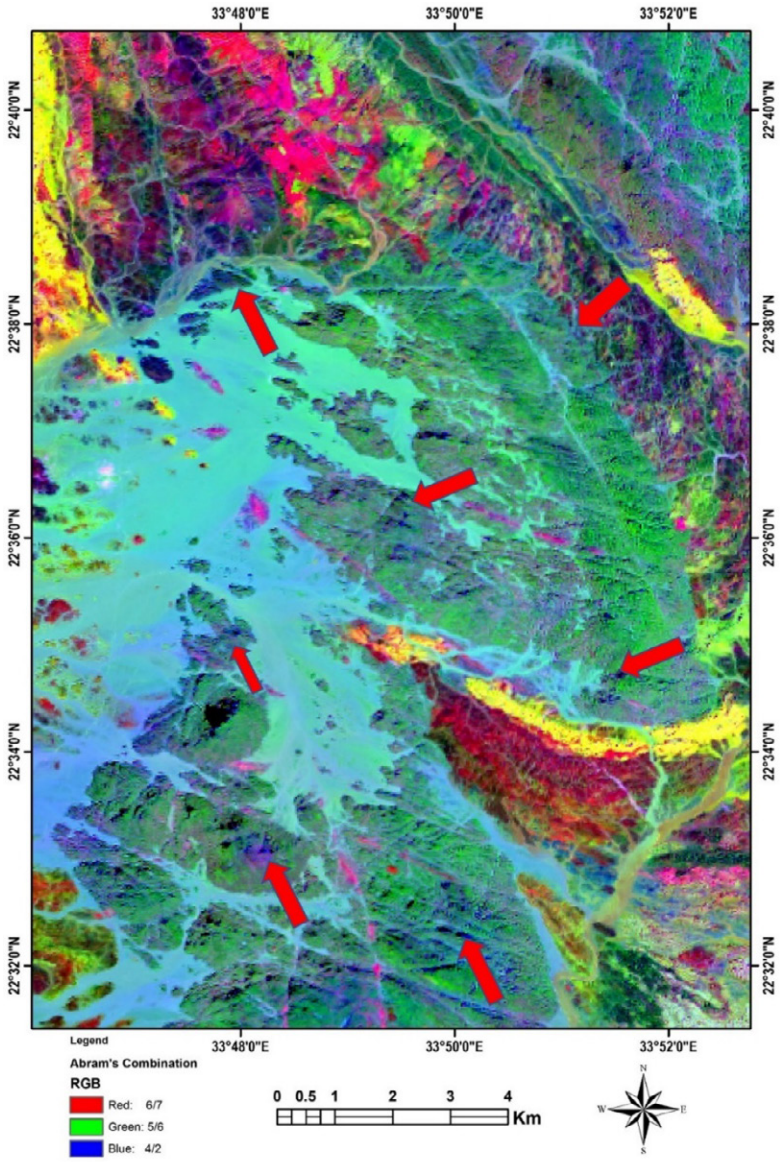

Figure 6: False color composite image for band ratios of (6/7), (5/6) and (4/2) in RGB, Um Ara - Um Shilman area, (SED) of Egypt.

image for these minerals [11,12,28-32].

As shown from the results of the principal component analysis (PCA) (Figure 7), the distribution of the lithologic rock units in the area of Um Ara – Um Shilman along with the statistical results showed that the best colour composites were created using PC3, PC2 and PC1 in RGB, which displayed good result for differentiate the fine grained alkali-feldspar granite at north Um Ara anomaly location. Both colour composite (PC4, PC3 and PC2 in RGB) and (PC5, PC3 and PC2 in RGB) exhibits additional clear discrimination areas along the study area in southern and eastern parts (yellow circles) (Figure 7). On the other hand, the combination of PC5, PC4 and PC3 in RGB showed the trachyte dyke intruded the granitic plutons of Um Ara at the middle and southern parts.

GIS techniques on North Um Ara trenches

The northern location of Um Ara has attracted attention for its high radioactive anomaly recorded during the field project accomplished by the Egyptian Nuclear Materials Authority since 1978. The uranium occurrences have been founded related to; fine to medium grained alkali-feldspar granite that located in the northern part of Um Ara granitic pluton in the oxidized zones; where the alteration has taken place in the rocks with the aid of the hydrothermal solutions which helped in uranium enrichment and remobilization [17,18,33].

The detailed exploration program of the Egyptian Nuclear Materials Authority that extend to the year 2000, aimed to follow radioactive mineralization and the alteration process with the depth over a length of 3.5 km by digging the sixteen trenches (Figure 8). Visible secondary uranium and violet fluorite mineralization appears along the joint and fracture planes and their intersection. The mineralization and intensity of alteration processes, increased with the increasing of the digging. These alteration processes act as a chemical trap for mineralization. (Table 1) shows the average values of radioelements measurements (TC, eU, eTh and K%) and the calculated ratios (eU/K, eU/eTh and eTh/K) for the trenches.

doi: 10.37532/gigs.2020.8(5).269

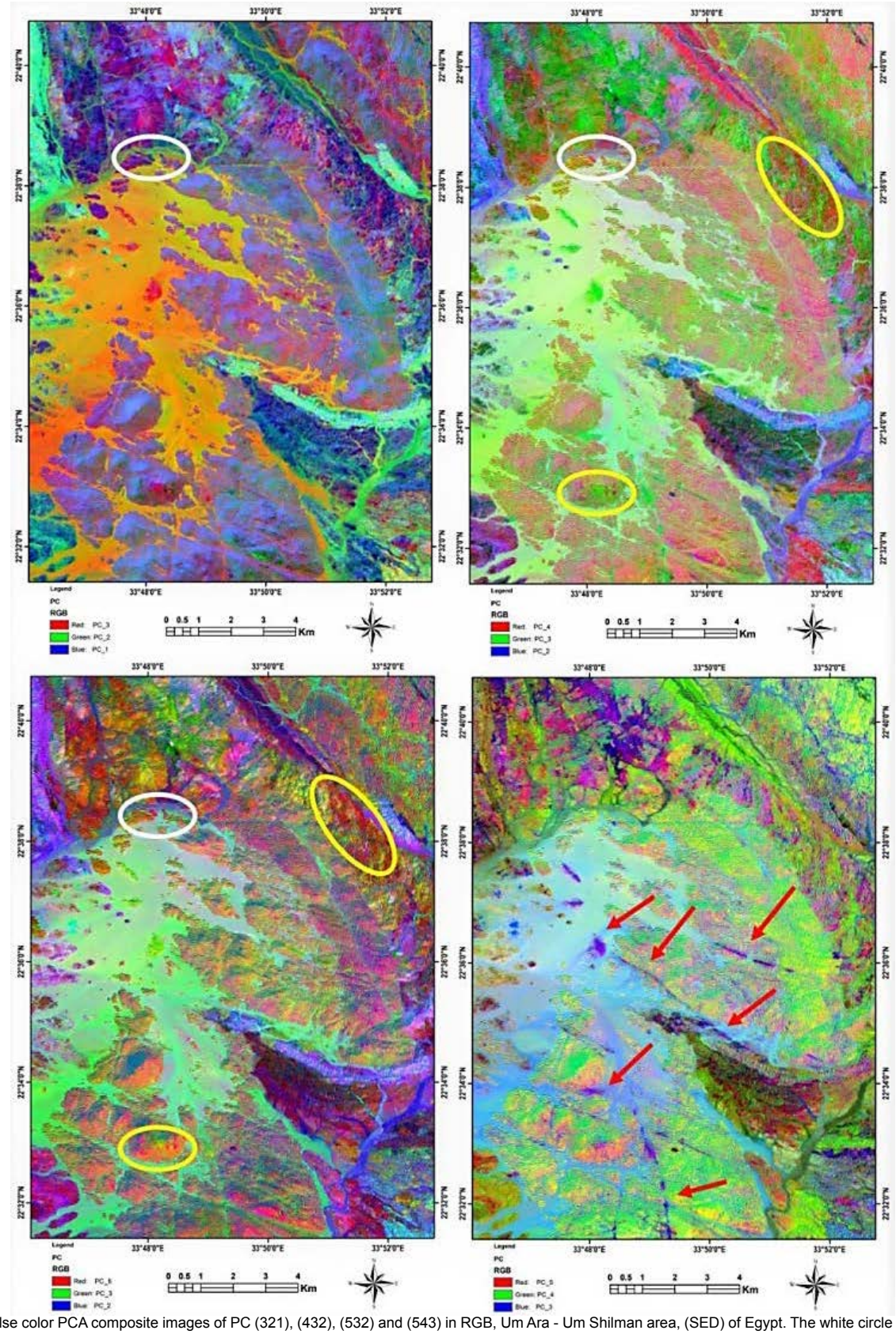

Figure 7: False color PCA composite images of PC (321), (432), (532) and (543) in RGB, Um Ara - Um Shilman area, (SED) of Egypt. The white circle shows the north Um Ara location, the yellow circles represent the promising locations. The red arrows show the trachyte dyke.

doi: 10.37532/gigs.2020.8(5).269

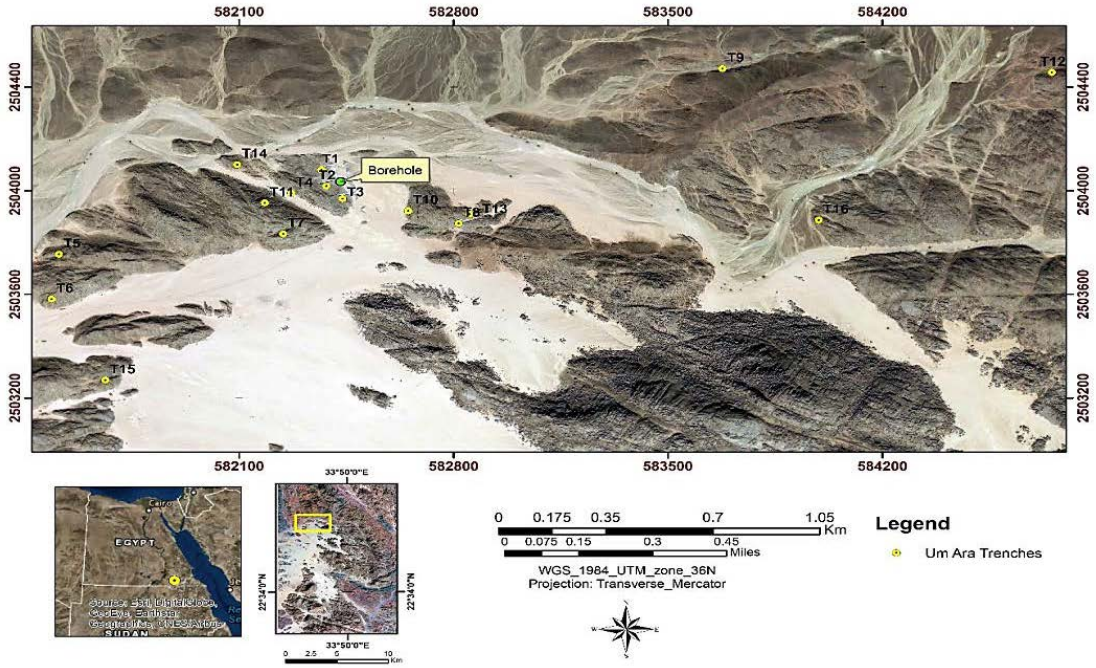

Figure 8: Northern Um Ara – Um-Shilman area trenches location and distribution, (SED) of Egypt.

Trench No.	North	East	Tc (Ur)	K%	eU(ppm)	eTh(ppm)	eU/K	eU/eTh	eTh/K
T1	2504081	582369	345.02	4.82	250.05	90.37	51.878	2.767	18.749
T2	2504018	582385	347.52	4.37	236.10	111.69	54.027	2.114	25.558
T3	2503969	582437	223.89	4.13	141.11	76.31	34.167	1.849	18.477
T4	2503991	582270	210.01	4.18	147.60	58.42	35.311	2.527	13.976
T5	2503755	581511	216.54	4.33	151.37	60.42	34.958	2.505	13.954
T6	2503582	581488	182.10	4.19	121.40	55.51	28.974	2.187	13.248
T7	2503834	582244	310.00	4.55	230.83	76.33	50.732	3.024	16.776
T8	2503874	582817	242.98	4.44	73.66	166.20	16.590	0.443	37.432
T9	2504472	583678	203.62	4.18	66.23	139.27	15.844	0.476	33.318
T10	2503923	582652	210.89	4.14	68.98	139.51	16.662	0.494	33.698
T11	2503953	582184	218.68	4.24	157.29	56.72	37.097	2.773	13.377
T12	2504457	584754	173.90	4.00	51.01	119.29	12.753	0.428	29.823
T13	2503910	582852	232.26	4.40	70.70	157.35	16.068	0.449	35.761
T14	2504101	582094	249.07	4.41	175.71	67.66	39.844	2.597	15.342
T15	2503269	581663	223.68	4.13	153.05	63.94	37.058	2.394	15.482
T16	2503887	583992	211.86	4.30	63.11	143.82	14.677	0.439	33.447

Table 1: The radioelements value measurements with ratios for the trenches at north Um Ara location, Um Ara - Um Shilman area, (SED) of Egypt.

Generalized classes based on the relative abundance and the spatial distribution of each radioelement has been mapped (Figure 9). The mapped sample values showed a relative quantity for each selected radioelement grouped into three classes. The classification method used was the Natural Break (Jenks) method. Mean and standard deviation were also calculated for each selected isotope. The uranium values located at the west trenches were founded higher than that located in the east trenches and vice versa for the thorium values. So, there are two groups of trenches; the first one is high in uranium and the second is high in thorium. The following is the description of the representative examples for these trenches with the radiometric distributions in ppm.

High Uranium Trenches (Nos.1, 2, 3, 4, 5, 6, 7, 11, 14 and 15)

In this group, the trench no. 1 (T1) is the representative trench. This trench has striking N50oE and its geological features, and dimensions are shown in Figure 9. Iron and manganese are alternated on both the two wall rock sides. The rock is highly sheared and jointed striking E-W and NW directions. The spectrometry's measurements (Tc, K%, eU, eTh) along the trench are contoured (Figure 10). Most the high eU and eTh are associated with violet fluorite.

There is a strong positive correlation between Tc with (K%, eU,

doi: 10.37532/gigs.2020.8(5).269

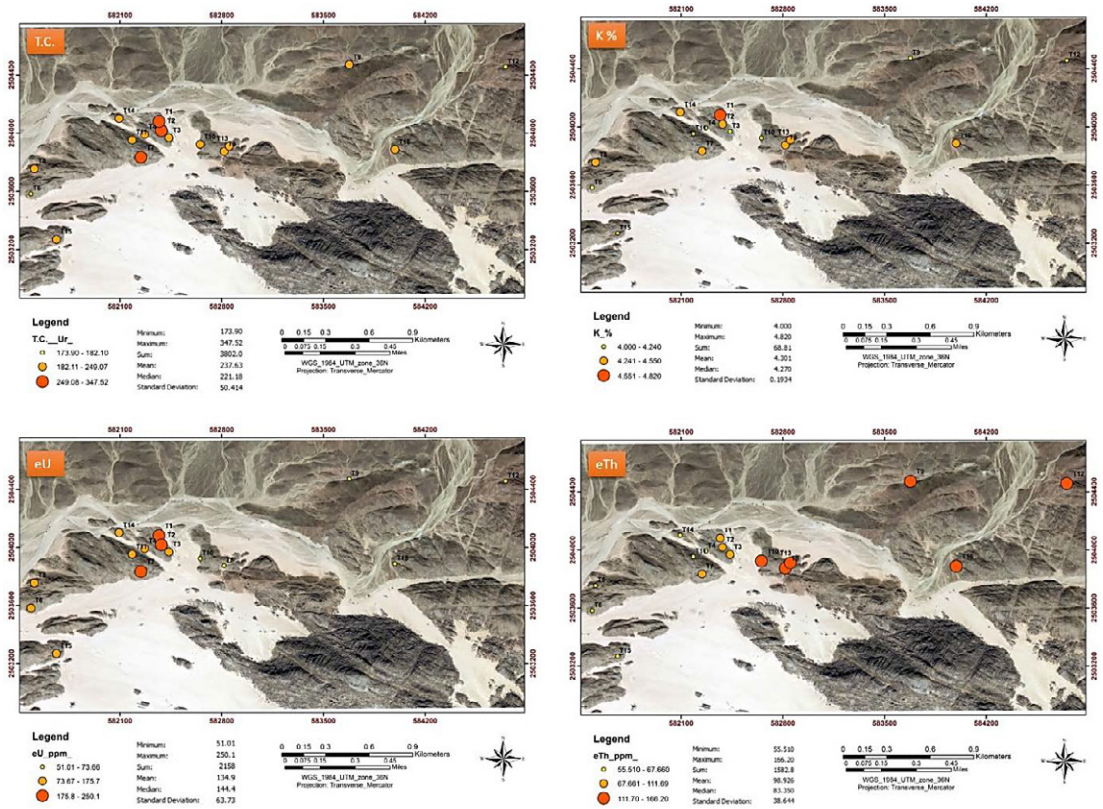

Figure 9: The spectrometry's measurements and its statistics for the trenches including (Tc), (K%), (eU) and (eTh), Um Ara - Um Shilman area, (SED) of Egypt.

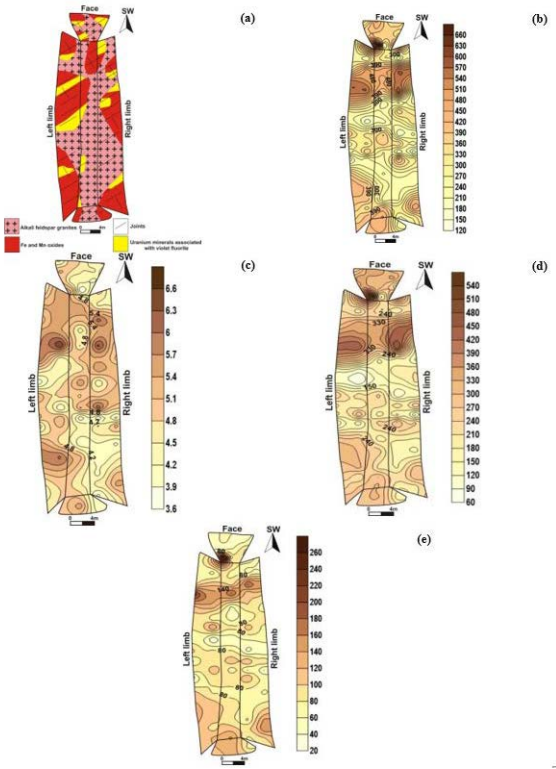

Figure 10: Representative view showing (a) the geological map as well as, (b) Total count (Tc), (c) K (%), (d) eU (ppm) and (e) eTh (ppm) concentration maps for trench No. 1 (high uranium), Um Ara - Um Shilman area, SED, Egypt modified after.

doi: 10.37532/gigs.2020.8(5).269

eTh) within all trenches of this group (Figure 11). The correlation between K%, with eU and eTh within the all trenches reflected the positive relation. On the other hand, there is a negative relation between eTh and eU/eTh. The relation between eTh and eU, illustrated that the all samples lie (eU/eTh ratio) between 10 to 1 value, and this confirmed by the correlation with mobility (eU-eTh/3.5) ratio, which reflected strong uranium mobilization, where all samples lies in the leaching field (Figure 11). The above correlation values indicated the direct relation between eU, eTh and K%.

High Thorium Trenches (Nos. 8, 9, 10, 12, 13 and 16)

Trench No. 16 (T16) is the representative trench for this group. This trench striking N and its geological features and dimensions are shown in Figure 12. The iron and manganese occur either as veinlet or as aggregates of fine-grained masses coated the all parts of the trench. The rock is dissected by jointing striking NW-SE and E-W directions. The spectrometry's measurements (Tc, K%, eU, eTh) along the trench are contoured (Figure 12). The high eTh-content is associated with Fe

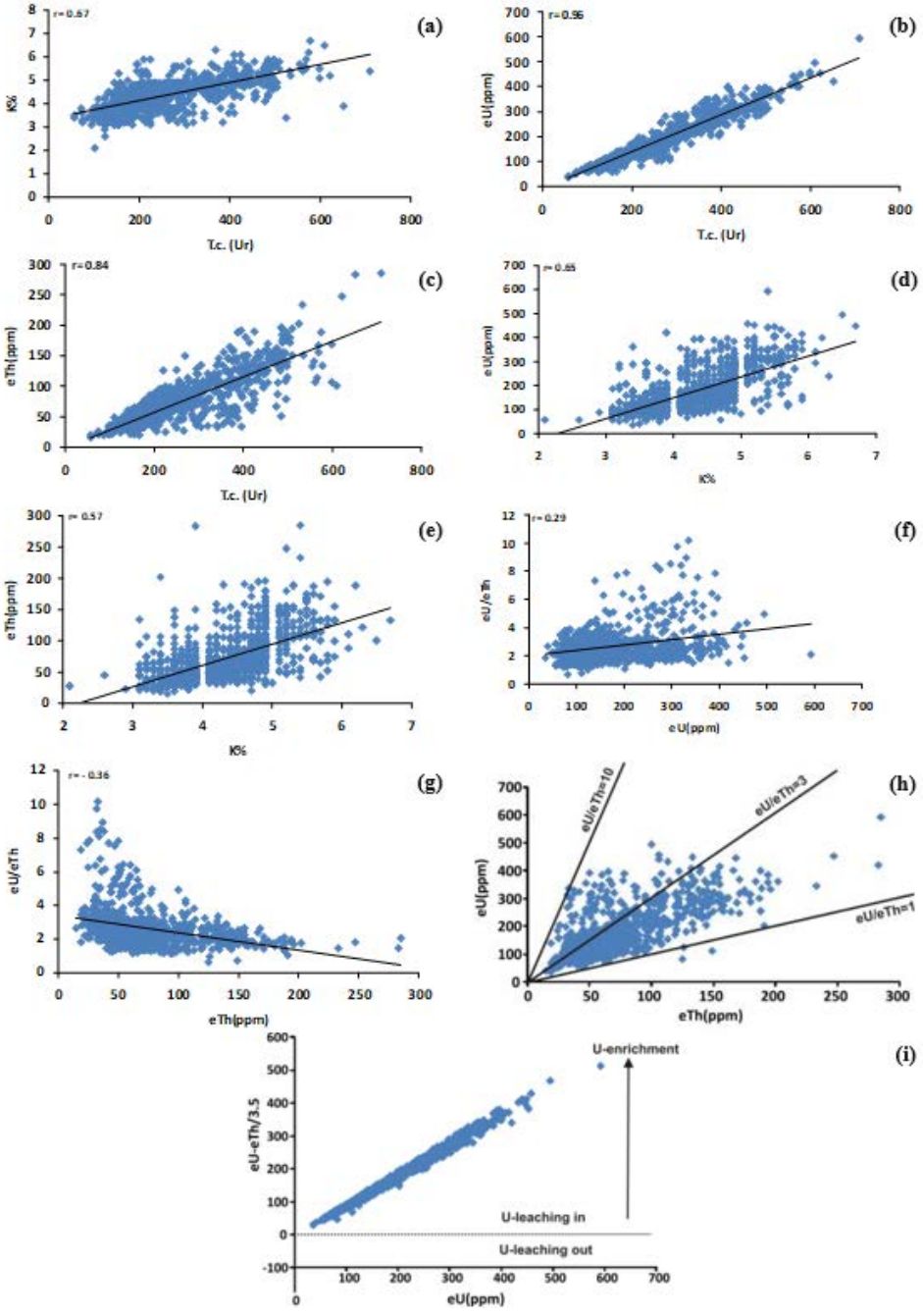

Figure 11: The relation between Tc (μr) vs. (a) K%, (b) eU and (c) eTh, K% vs. (d) eU and (e) eTh, (f) eU vs. eU/eTh, (g) eTh vs. eU/eTh, (h) eTh vs. eU and (i) eU vs. eU-eTh/3.5, along trenches high uranium (Nos. 1, 2, 3, 4, 5, 6, 7, 11, 14 and 15) at Um Ara - Um Shilman area, SED, Egypt.

doi: 10.37532/gigs.2020.8(5).269

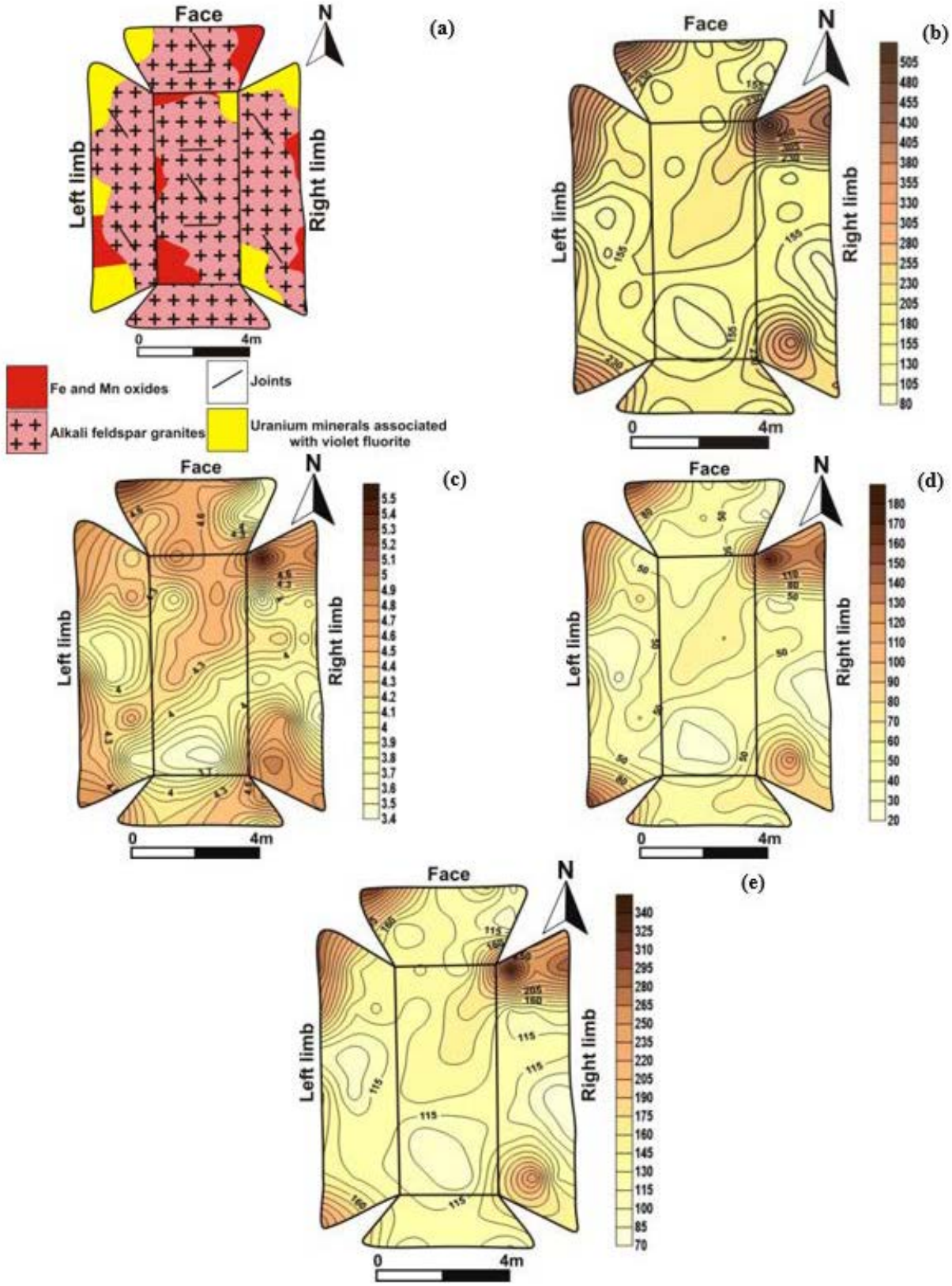

Figure 12: Representative view showing (a) the geological map as well as, (b) Total count (Tc),(c) K (%), (d) eU (ppm) and (e) eTh (ppm) concentration maps for trench No. 16 (high thorium), Um Ara - Um Shilman area, SED, Egypt modified after.

doi: 10.37532/gigs.2020.8(5).269

and Mn-dendrites.

The correlation between Tc with (K%, eTh, eU) within the all trenches of high thorium had a strong positive relation (Figure 13). Also, the correlation between K%, with eU and eTh within the all trenches had a positive relation. While, the relation between eU and eTh with eU/eTh had a moderate positive relation. The correlation between eU and eTh, illustrated that all samples lie around (eU/eTh ratio) 0.5. The correlation between mobility (eU-eTh/3.5) and eU

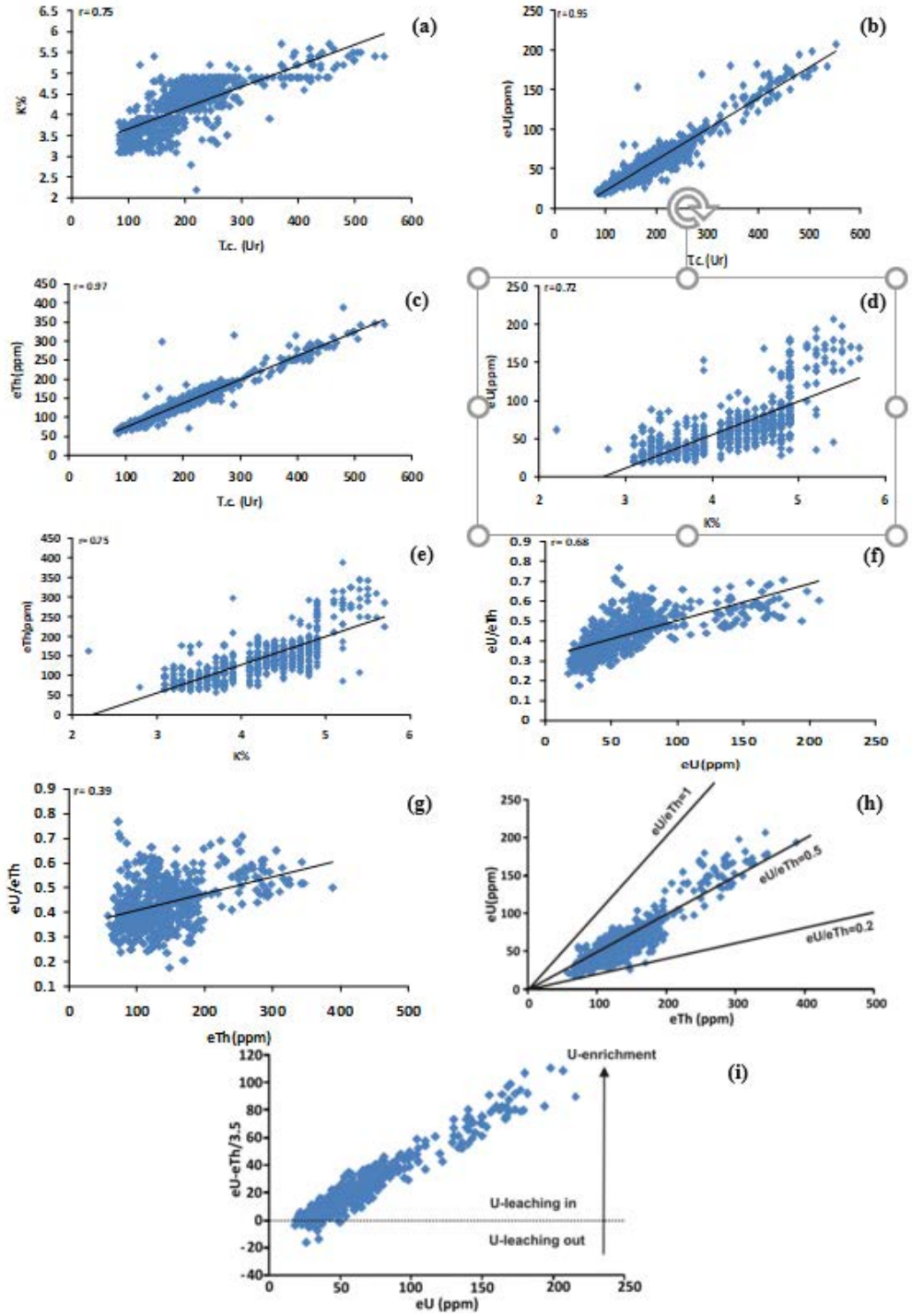

Figure 13: The relation between Tc (μr) vs. (a) K%, (b) eU and (c) eTh, K% vs. (d) eU and (e) eTh, (f) eU vs. eU/eTh, (g) eTh vs. eU/eTh, (h) eTh vs. eU and (i) eU vs. eU-eTh/3.5, along trenches high thorium (Nos.8, 9, 10, 12, 13 and 16) at Um Ara - Um Shilman area, SED, Egypt.

within the all trenches reflected uranium mobilization.

The three auxiliary variables, namely: the two element ratios (eU/K%, eU/eTh and eTh/K%) were computed and mapped using the natural neighbour interpolation method (Figure 14), in order to represent the spatial distribution of the variables. So as to establish the degree of uranium mobilization, and consequently to know the areas affected by this remobilization, it is favourable to studying the uranium and thorium concentrations and their ratios [34-36]. According to Fouad, Rabie and Khalil [35], the uranium is not redistributed in two cases; when there are not sufficient solutions that needed for uranium remobilization, or the essential uranium amount is located in particular resistant stable lithologic units, where it is obviously indicated by the negative increase of eU/eTh ratio with the increase of eU. In the case of the present study area, there is an observable increase in ratio eU/eTh with the increase in eU values (Figure 15) which reflected uranium redistribution and re-concentration. The inverse proportionality between eU/eTh and eTh indicated the possibility of forming uranium ores, particularly if the rocks are characterized by high eU/eTh (Figures 14 and 15).

Efimov [37] proposed F-alteration indicator (Figure 14) for giving information about rock alteration by the following relationship:

$$F = \frac{eU}{eTh/eU} = \frac{eU}{eTh/K} = \frac{eU * K}{eTh}$$

The F-alteration indicator is significant for including two specific features about rock environment; the first is the potassium abundance to the ratio of eTh/eU, the second is the uranium abundance to the ratio of eTh/K. The F-parameter map is useful to locate a zone of strong K alteration associated with the uranium mineralization.Two various composite colour image maps "ternary radioelement map" were also produced for the following variable combinations (Figure 16).

eU, K% and eTh as RGB respectively three radioelements composite colour image map.

eU, eU/K% and eU/eTh as RGB respectively three radioelements composite colour image map.

The "ternary radioelement map" is a type of image mapped to the ground using a combination of the three-radioelement false colour images. This image is a transform of three radioelement concentrations plotted on a triangle, where each apex represents the maximum concentration of each radioelement, with concentrations decreasing to the minimum along a scale perpendicular to the apex. The maximum value for each radioelement, eU, K and eTh, is assigned a colour – red, green and blue, respectively, as standardized for the display of gamma ray spectrometry data [11,38,39]. Because of the association of potassium with particular minerals and therefore rock types, the overlay of ternary radio element data on a false colour

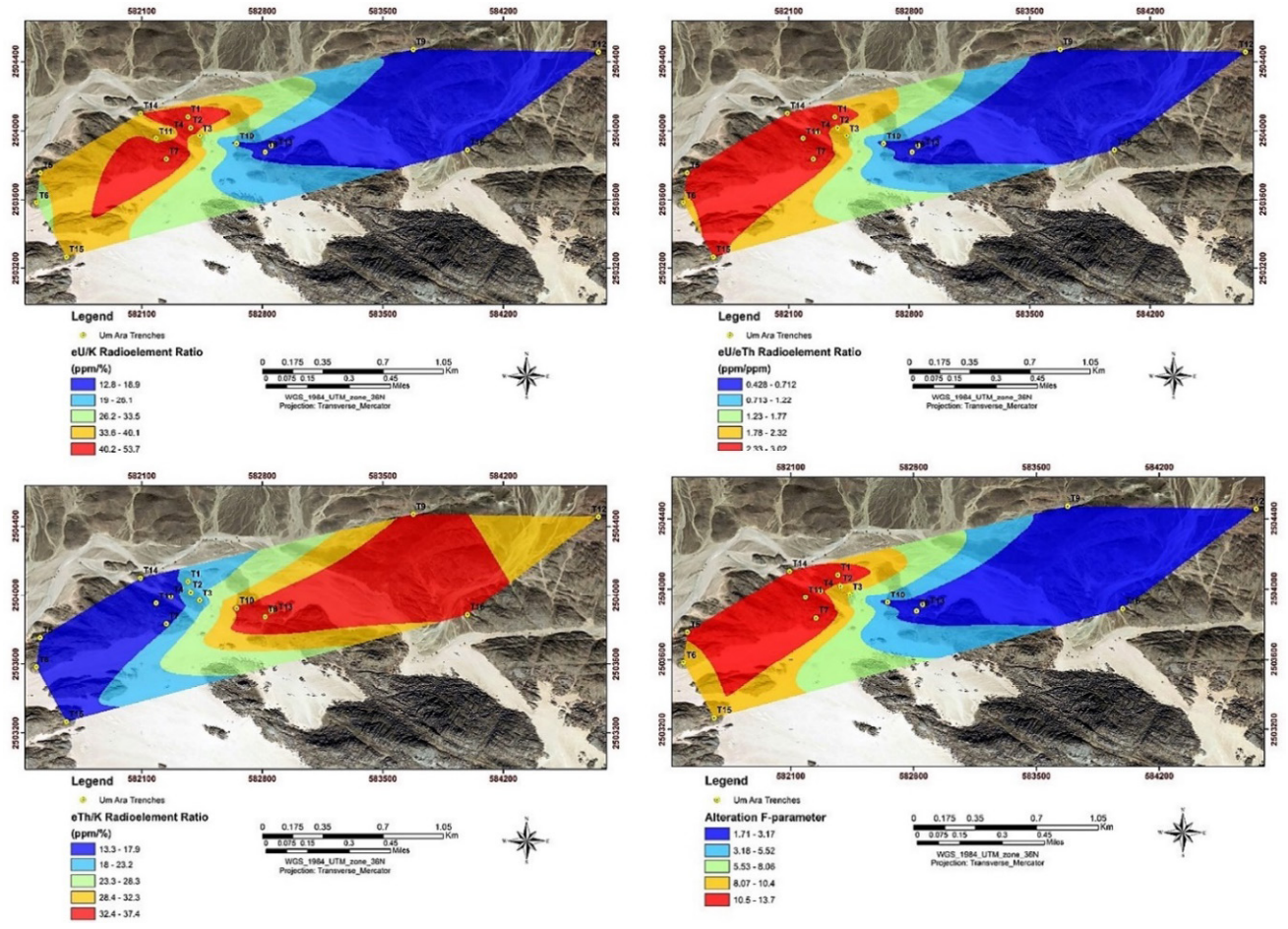

Figure 14: Interpolated maps showing the spatial distribution of the radioelement's ratios,Um Ara - Um Shilman area, (SED) of Egypt.

doi: 10.37532/gigs.2020.8(5).269

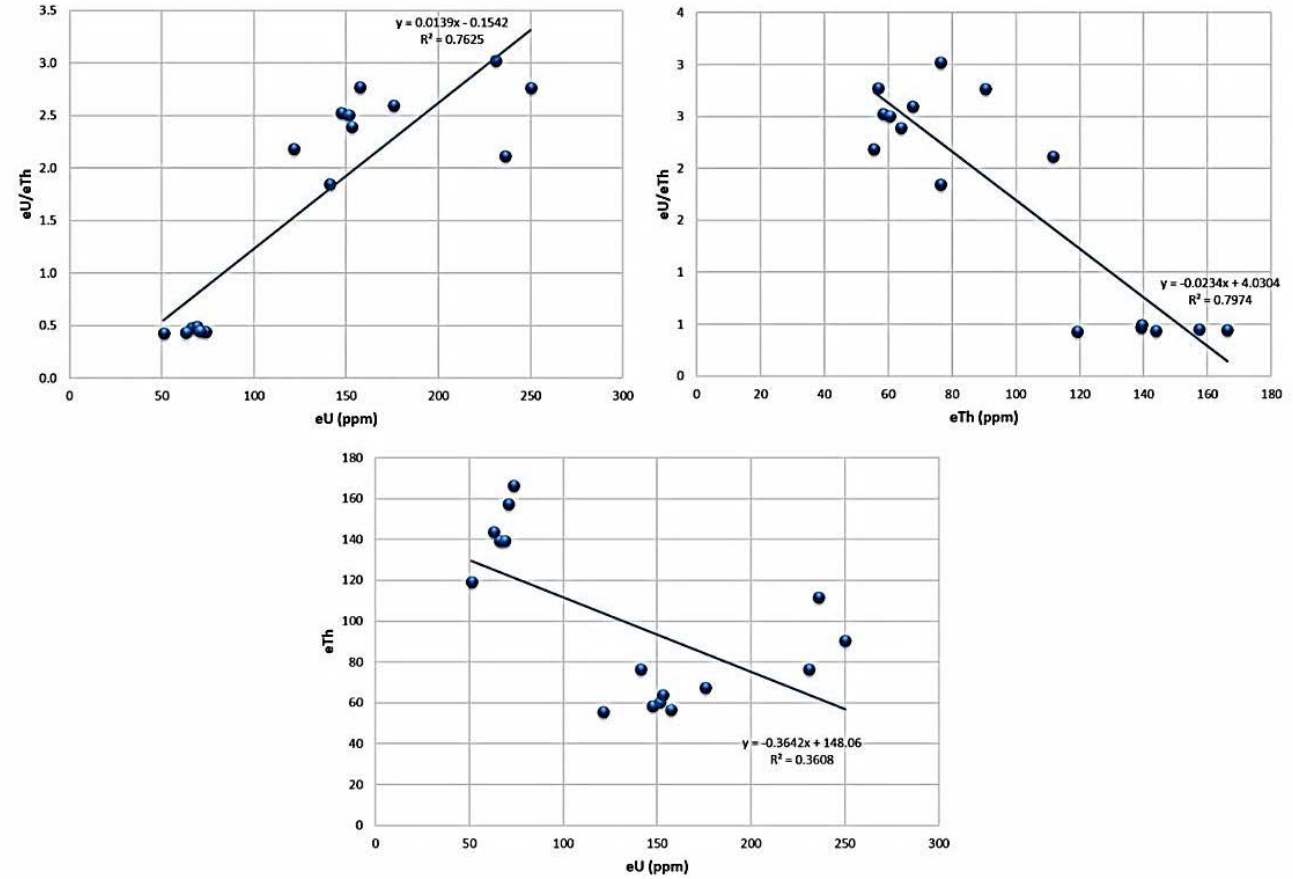

Figure 15: Binary radioelements relationships,Um Ara - Um Shilman area, (SED) of Egypt.

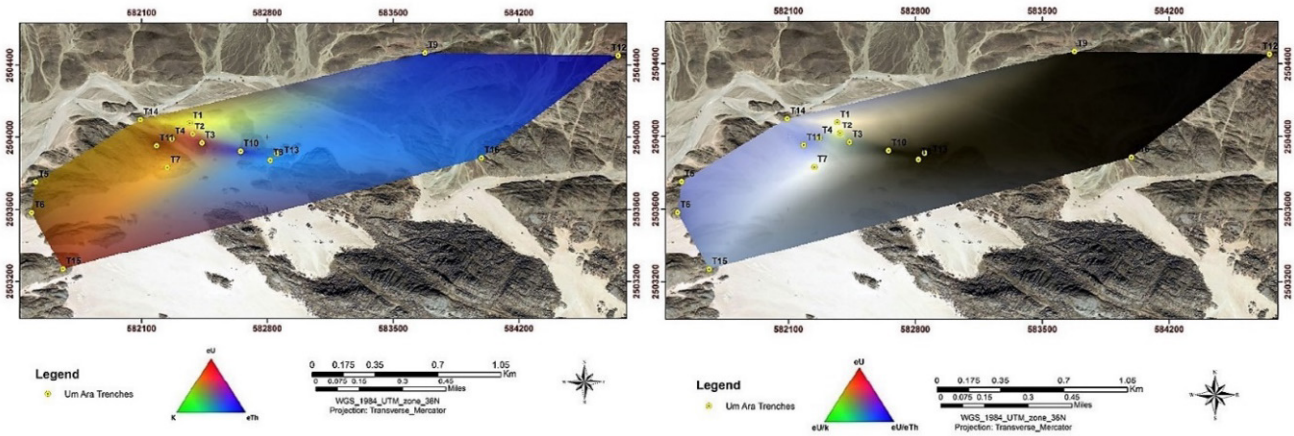

Figure 16: Ternary composite radioelement images, namely: eU, K and eTh in RGB (left); eU, eU/K and eU/eTh in RGB respectively (right),Um Ara - Um Shilman area, (SED) of Egypt.

image map enhanced the potential for lithologic discrimination based on colour differences.

Figure 17 showed the uranium leaching according to the relation between the uranium and thorium abundances in the rock. When eU-eTh/3.5 increases that means uranium re-concentration, while if there are passive increase values means uranium leaching out from the rock. As shown in the figure the uranium leached in the western area where there is an altered alkali feldspar granite

Conclusions

The study area lies in the extreme south Eastern Desert of Egypt and geologically comprises metavolcanics and Dokhan volcanism that

doi: 10.37532/gigs.2020.8(5).269

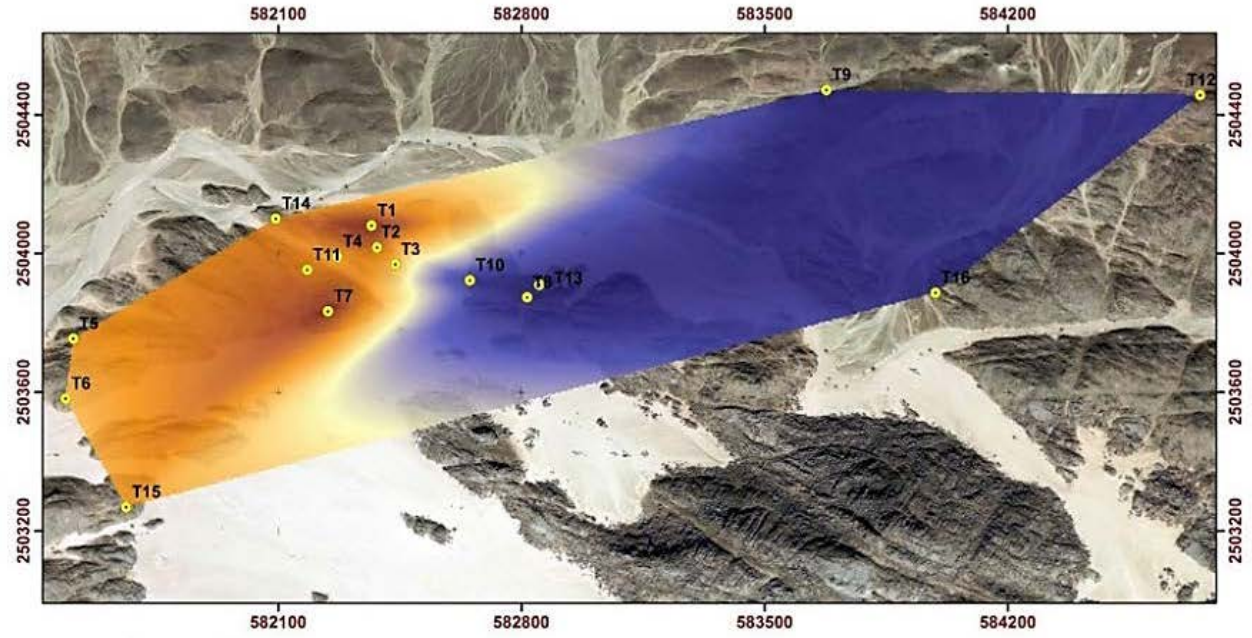

Legend

Um Ara Trenches

Uranium Leaching

eU-eTh/3.5

Leaching In

Leaching Out

0 0.175 0.35 0.7 1.05 Km

0 0.075 0.15 0.3 0.45 Miles

WGS_1984_UTM_zone_36N
Projection: Transverse_Mercator

Trench No.	eU-eTh/3.5
T1	45.62
T7	44.14
T2	35.55
T14	30.87
T11	28.73
T5	25.99
T4	25.48
T15	25.46
T6	18.83
T3	18.51
T12	-19.51
T10	-20.15
T9	-20.87
T16	-23.06
T13	-24.76
T8	-26.44

*** Red = U-Leaching Out*
Green = U-Leaching In

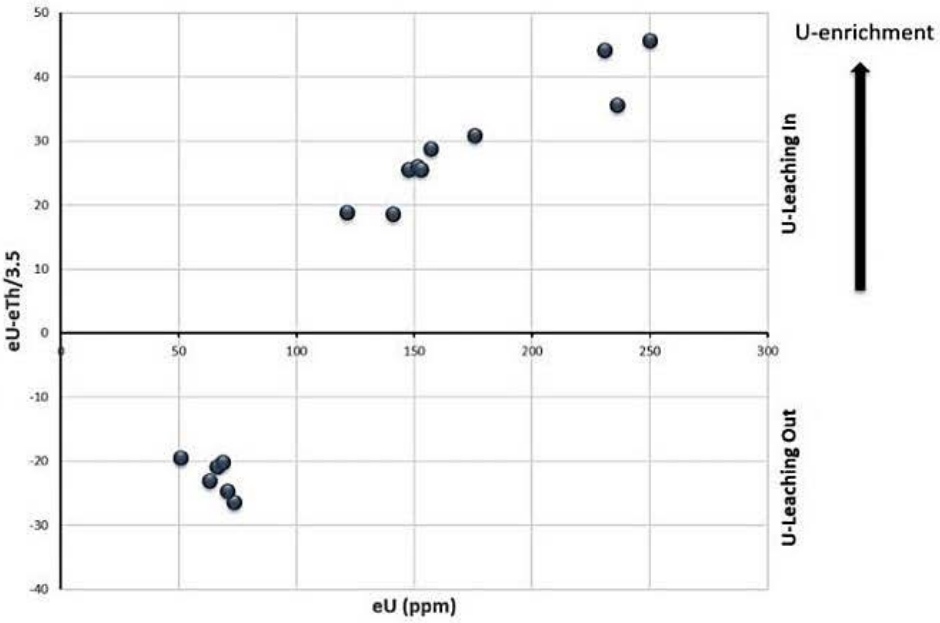

Figure 17: Uranium leaching analysis for the measured trenches of north Um Ara - Um Shilman area, SED, Egypt.

were intruded by the younger granites. These granites are classified into monzogranite and alkali-feldspar granite. The monzogranite is coarse-grained with an oval-shaped pluton trending N–S to NW–SE. The alkali-feldspar granite is emplaced at the northern contact of the Um-Ara – Um Shilman monzogranite rock. It is fine to medium-grained, reddish-pink to red in colour and sends apophyses and off shoots into the northern Dokhan volcanic of G. Um Dubr. It affected by hydrothermal activities, which manifested by thematicization, silicification with partial kaolinization together with the frequent presence of manganese oxides, green and violet fluorite and uranium mineralization (uranophane and soddyite).

The study conducted an investigation using Landsat 8 OLI level 1T radiance at sensor data and remote sensing techniques to map the lithologic units and the alteration zones in Um Ara – Um Shilman at South-eastern Desert of Egypt. Analysis and interpretation of Landsat 8 OLI were using false colour images of band combination, decorrelation stretching, band ratios and PCA, in order to differentiate lithologic units and altered rocks associated with uranium occurrences. The composite image, decorrelation stretching enhancement transform and PCA techniques showed clearly the boundaries of the lithologic units in the area and represented the ability to differentiate between the target fertile alkali-feldspar granite and the less important monzogranite rock unit, regarding its enrichment of the uranium mineralization. Band ratios technique showed the distribution of the alteration zones in a large-scale area of investigation.

A detailed radioelement measurement has been acquired from a local area located at the northern part of Um Ara granitic pluton, where it faulted against the younger Dokhan volcanic rock unite to the north. The uranium mineralization founded associated with the fine to medium grained alkali-feldspar altered granite. Sixteen trenches have been dug with radioelements measurements. The radioelements ratios and colour composite pseudo images methods used in a GIS environment with the suitable interpolation method applied, represented a powerful tool for extracting useful information on the uranium occurrences and remobilization in the area. The outcome results showed that the uranium re-concentrated in the area related to the alkali-feldspar granitic type rock, which allowed an accumulation for uranium ores in these particular locations. From the eU-eTh/3.5 ratio, uranium leached in the western area where there is an altered alkali-feldspar granite.

Acknowledgements

The authors are deeply indebted to Prof. Dr. Mahmoud Hany Shalaby, Nuclear Materials Authority, Egypt, for critically reading the manuscript, numerous helpful, valuable and constructive comments which lead to improve the original version of the manuscript.

References

1. Stern R, Hedge C (1985) Geochronologic and isotopic constraints on late Precambrian crustal evolution in the Eastern Desert of Egypt. American Journal of Science 285:97-127.
2. Gaby S (1975) Petrochemistry and geochemistry of some granites from Egypt. Neues Jahrbuchfur Mineral 124:147-189.
3. Akaad M, Noweir A (1980) Geology and Lithostratigraphy of the Arabian Desert Orogenic belt of Egypt between latitudes 25° 35' and 26° 30' N. Inst. App. Geol. Bull.3:127-136.
4. Hassan M, Hashad A (1990) Precambrian of Egypt.The Geology of Egypt. Balkema, Rotterdam: 201-245.
5. Kröner A, Krüger J, Rashwan A(1994) Age and tectonic setting of granitoid gneisses in the Eastern Desert of Egypt and south-west Sinai. Geologische Rundschau 83:502-513.
6. Beyth M, Stern J, Altherr R, Kröner A (1994) The late Precambrian Timna igneous complex, southern Israel: evidence for comagmatic-type sanukitoidmonzodiorite and alkali granite magma. Lithos 31:103-124.
7. Rowan L, Schmidt R, Mars J (2006) Distribution of hydrothermally altered rocks in the Reko Diq, Pakistan mineralized area based on spectral analysis of ASTER data. Remote Sensing of Environment 104:74-87
8. Mars C, Rowan C (2011) ASTER spectral analysis and lithologic mapping of the Khanneshin carbonatite volcano, Afghanistan. Geosphere 7:276-289.
9. Akbari Z, Rasa I, Mohajjel M, Adabi M (2015) Hydrothermal Alteration Identification of Ahangaran Deposit, West of Iran Using ASTER Spectral Analysis. International Geoinformatics Research and Development Journal.6.
10. Gupta R (2003) Remote Sensing Geology, 2nd edition. Heidelberg, Springer, Berlin pp. 655
11. Arafy R (2016) Discrimination of various rock units in Abu Zenima area, Southwestern Sinai, Egypt, with emphases to the radioactive areas using the hyperspectral remote sensing and GIS techniques. The University of Alabama at Birmingham.
12. Zalaky A, Essam M, Arafy A (2018) Assessment of Band Ratios and Feature-oriented principal component selection (FPCS) Techniques for Iron Oxides Mapping with relation to radioactivity using Landsat 8 at Bahariya Oasis, Egypt. Researcher.10: 10.
13. Amara B, Aissa D, Maouche S, Braham M, Machane D (2019) Hydrothermal alteration mapping and structural features in the Guelma basin (Northeastern Algeria): contribution of Landsat-8 data. Arabian Journal of Geosciences 12:94.
14. Ali A, Pour A (2014) Lithological mapping and hydrothermal alteration using Landsat 8 data: a case study in ariab mining district red sea hills Sudan. Int. Journal of Basic and Applied Sciences 3:199-208.
15. Aryanmehr H, Hosseinjanizadeh M, Honarmand M, Naser F (2018) Hydrothermal alterations mapping using Quickbird and Landsat-8 data, a case study from Babbiduyeh, Kerman province, Iran. Journal of Mining and Environment 9:41-52.
16. Conoco C (1987) Geological map of Egypt, scale 1: 500,000-NF 36 NE-Bernice, Egypt. The Egyptian General Petroleum Corporation, Cairo.
17. Abdel Meguid A (1986) Geologic and radiometric studies of uraniferous granite in Um Ara-UmShilman area, south Eastern Desert, Egypt. Suez Canal University, Egypt.
18. Ibrahim ME (1986) Geologic and radiometric studies on UmAra granite pluton, south east Aswan, Egypt. Monsoura University, Egypt.
19. Abdalla H (1996) Geochemical and mineralogical studies at Um Ara rare metals prospect, southeastern Desert, Egypt. PhD Thesis, Hokkaido University.
20. Saleh G, Kamar M (2018) Geochemical Characteristics and Radioactive Elements Estimation along Trenches of Um Ara area, South Eastern Desert, Egypt. Geoinformatics & Geostatistics: An Overview 6.
21. Saleh G (2002) Neoproterozoic volcanism at Um Shilman-Um Dubr area, Southeast Aswan, Egypt: geology, geochemistry and tectonic environment of the Dokhan Volcanic Formation. Neues Jahrbuchfür Mineralogie-Abhandlungen: Journal of Mineralogy and Geochemistry 177:321-347.
22. Sibson R (1981) A brief description of natural neighbour interpolation. chapter 2 in Interpreting Multivariate Data, New York: John Wiley & Sons:21–36.
23. Madani A, Emam A (2011) SWIR ASTER band ratios for lithological mapping and mineral exploration: a case study from El Hudi area, southeastern desert, Egypt. Arabian journal of Geosciences 4:45-52.
24. Pournamdari M, Hashim M, Pour AB (2014) Spectral transformation of ASTER and Landsat TM bands for lithological mapping of Soghan ophiolite complex, south Iran. Advances in Space Research 54:694-709.
25. Vincent R (1997) Fundamentals of Geological and Environmental Remote Sensing: Upper Saddle River, NJ: Prentice-Hall, Inc.
26. Yamaguchi Y, Naito C (2003) Spectral indices for lithologic discrimination and mapping by using the ASTER SWIR bands. International Journal of Remote Sensing 24:4311-4323.

27. Sabins F (1999) Remote sensing for mineral exploration. Ore Geology Reviews 14:157-183.

28. Loughlin W (1991) Principal Component Analysis for alteration mapping. Photogrammetric Engineering and Remote Sensing 57:1163-1169.

29. Crosta A, Moore J (1989) Enhancement of Landsat thematic mapper imagery for residual soil mapping in SW Minais Gerais atate, Brazil: a prospecting case history in Greenstone belt terrain, in: proceedings of the Seventh ERIM Thematic Conference. Remote sensing for Exploration Geology:1173-1187.

30. Khaleghi M, Ranjbar H, Shahabpour J, Honarmand M (2014) Spectral angle mapping, spectral information divergence, and principal component analysis of the ASTER SWIR data for exploration of porphyry copper mineralization in the Sarduiyeh area, Kerman province, Iran. Applied Geomatics 6:49-58.

31. Kwarteng A and Chavez J (1989) Extracting spectral contrast in Landsat Thematic Mapper image data using selective principal component analysis. Photogrammetric Engineering and Remote Sensing 55:339-348.

32. Crosta A, Azevedo F, Brodie C (2003) Targeting key alteration minerals in epithermal deposits in Patagonia, Argentina, using ASTER imagery and principal component analysis. International Journal of Remote Sensing 24:4233-4240.

33. El-Naby A (2009) High and low temperature alteration of uranium and thorium minerals, Um Ara granites, south Eastern Desert, Egypt. Ore Geology Reviews 35:436-446.

34. Mansour S, EL-Afandy A, Abdalla H, Saleh G (2000) Uranium potentiality of Um Ara area, Southeastern Desert, Egypt. Internal Report, Nuclear Materiales Authority, Cairo, Egypt. Nuclear Materiales Authority, Cairo, Egypt

35. Fouad K, Rabie S, Khalil A (1998) Recognition of the Degree of Remobilization of Uranium from Airborne Gamma-Ray Spectrometric Survey Data: Proceeding of the Fourth Arab Conference on the Peaceful Uses of Atomic Energy.3

36. Asfahani J, Al-Hent R, Aissa M (2016) Uranium remobilization and migration evaluation through aerial spectrometric gamma technique in Syrian Desert (Area-1), Syria. Applied Radiation and Isotopes 107:278-292.

37. Efimov A (1978) Multiplikativnyjpokazateldljavydelenijaendogennychrud po aerogamma-spektrometriceskimdannym. Metodyrudnojgeofiziki. Leningrad, Naucno-proizvodstvennojeobjedineniegeofizika.

38. International Atomic Energy Agency (2003) Guidelines for radioelement mapping using gamma ray spectrometry data. IAEA. Technical Report Series.1363,

39. Abdelmohsen G, Arafy E, Mohammad G, Abdeen S (2019) Use of Remote Sensing and Gamma Ray Spectrometric Data for Elucidating Radioactive Mineralized Zones, Wadi Jararah-Wadi Kharit Area, South Eastern Desert, Egypt Global Journal of Science Frontier Research: (H) Environment & Earth Science 19:55-73.

Author Affiliation

Top

Department of EconomicGeology, Research Sector of GeologyNuclear, Materials Authority, Cairo, Egypt.